Romanian Reports in Physics, Vol. 59, No. 2, P. 357–375, 2007

Dedicated to Prof. Dorin N. Poenaru's 70th Anniversary

RADII OF HALO STATES IN LIGHT NUCLEI DEDUCED FROM ANC

F. CARSTOIU[1], L. TRACHE[2], C.A. GAGLIARDI[2], A.M. MUKHAMEDZHANOV[2], R.E. TRIBBLE[2]

[1] *National Institute for Nuclear Physics and Engineering*
P.O. Box MG-6, RO-077125 Bucharest-Magurele, Romania
E-mail: carstoiu@theory.nipne.ro
[2] *Cyclotron Institute, Texas A&M University, College Station, TX-77843, USA*
E-mail: trache@tamu.edu

(Received March 7, 2007)

Abstract. The experimental asymptotic normalization coefficients determined from peripheral transfer and breakup reactions are used to calculate the rms radius for proton or neutron halo states in some light nuclei ranging from ^{8}B to ^{21}Na (^{8}B,^{17}F, ^{17}O, ^{11}Be, ^{13}C, ^{15}C, and ^{21}Na). The procedure is applied to several ground and excited states, and it is shown that halo states, characterized by a rms radius of the last nucleon twice larger than that of the core, appear only for a favorable combination of low binding energy, and low or no Coulomb and centrifugal barriers. The influence of each of these three factors is considered on these selected cases.

Key words: halo states, drip line, asymptotic normalization coefficient.

1. **INTRODUCTION**

In the β stability valley, the proton root-mean square radii are precisely known for stable nuclei [1, 2] via the charge radii measured by electromagnetic interactions. The neutron rms radii are less known because they have been determined by strongly interacting probes whose interactions with nuclei must be phenomenologically modeled. A precise measurement of the neutron density radius would place an important constraint on the equation of state for neutron matter [3].

Much effort was dedicated in the recent years to the study of nuclei away from the β stability valley. This includes lifetimes, nuclear sizes, shell structure, excited states and decay modes. Frequently the one nucleon separation

energy is small, of the order of 1 MeV or less. This lead to a wealth of phenomena including soft collective modes, exotic transitions between low-lying states, changes in shell structure, long tails in density distributions, and most dramatically halo states [4, 5, 6, 7]. Compared to more stable nuclei, the increased size of the halo nuclei is strongly influenced by the smallness of the one (or two) nucleon separation energy, the Coulomb barrier and the angular momentum content of the ground state. Sometime, questions about possible unknown factors were raised, in particular after the discovery of two-neutron halo nuclei like ^{11}Li and ^{14}Be.

In one particle removal reactions involving weakly bound nuclei, the parallel and transverse momentum distributions of core like fragments are narrow compared with those of normal nuclei [7, 8], indicating increased nuclear size. The total reaction (interaction) and breakup cross sections are large, also reflecting the increased nuclear size. Furthermore, the increased density in the tail leads to a competition between the refractive power of the real part of the optical potential and the increased absorption due to the imaginary part. If the absorption at the barrier is dominant, then we are in a strong absorption regime, which provides a favorable window for the ANC (Asymptotic Normalization Coefficient) method to be discussed in this paper. Therefore these three processes have been proposed to extract informations on nuclear sizes. The Glauber theory in the optical limit has been proposed to extract nuclear sizes [9, 10, 11, 12]. This technique still needs to be improved in order to include properly Pauli blocking and finite range effects. When the widths of the measured parallel momentum distributions are related to the size of the spatial wave function of the last nucleon, complications arise from the reaction model used, and therefore, most of these determinations of nuclear radii are model dependent.

In Ref. [13] we proposed to use the experimental asymptotic normalization coefficient (ANC) to determine the rms radius of halo or weakly bounded nuclear states and have shown that the method provides the most reliable, least model dependent evaluation of this important quantity. In that paper, the ANC specifying the amplitude of the tail of the ^{8}B many-body wave function projected on the two body channel ^{7}Be+p, determined from transfer reactions [14], was used to calculate the rms radius for the ground state of ^{8}B and it was shown to be a proton halo nucleus. We showed that for the case of halo nuclear states, the asymptotic region has the dominant contribution to observables favoring large distances from the core, like the mean square radius, and that therefore, the ANC is the quantity that can be best extracted from experiment and is the most relevant. In particular, we showed that the use of the ANC gives a reliable and model independent experimental value for the rms radius of the ^{8}B halo. The result does not depend on particular

assumptions made about the configuration of the state, or on the shape or the parameters of the core-proton potential, not even on the assumption that such a potential (mean field) description is valid in the interior of the nucleus. This might become particularly important for light nuclei in which cluster phenomena are important, and for nuclei close to the drip lines, for which we cannot say a priori what mean field potential is appropriate, what shape and what terms may contain. This was due both to the large radial extension of the halo states and to the nature of the operator that favors contributions from larger distances. In order to illustrate and check this statement, in the present paper we apply the same procedure to a variety of nuclei. To see the influence of the three factors determining the halos we selected several nuclear states for which the ANC is known or can be determined from a variety of transfer reactions and determined their rms radii. These are either proton or neutron states, have different nucleon binding energies, different centrifugal barriers (s, p or d states) and different Coulomb barriers. The states under consideration are in the light nuclei ^{8}B,^{17}F, ^{17}O, ^{11}Be, ^{13}C, ^{15}C, and ^{21}Na. In Section 2 of the paper we review the basics of the method we use, in Section 3 treat the individual cases in detail, in Section 4 we discuss qualitatively the behaviour of proton halos at zero energy and summarize the conclusions in Section 5.

2. DESCRIPTION OF THE METHOD: RMS RADII OF HALOS FROM EXPERIMENTAL ANC

The nuclei are fermionic many-body quantum systems, their full wave function is complicated and therefore their complete description is a difficult task. Information obtained through experiments is related to the full wave function or to part of it, depending of the type of observables we measure, and should always be interpreted accordingly. We shall restrict ourselves to the case of nuclear reactions where the core survives, like in one-nucleon transfer reactions or one-nucleon removal reactions, and where, therefore, the matrix elements involve the overlap integral of the state wave functions for particles A, p, and B, where $B = (Ap)$ is a bound state of nucleus A and nucleon p, as given by [15, 16]:

$$I^B_{Ap}(\vec{r}) = \langle \mathcal{A}[\varphi_A(\xi_A)\varphi_p(\xi_p)]|\varphi_B(\xi_A,\xi_p,\vec{r})\rangle = \sum_{l_B,m_{l_B}j_Bm_{j_B}} \langle J_AM_Aj_Bm_{j_B}|J_BM_B\rangle$$

$$\times\langle J_pM_pl_Bm_{l_B}|j_bm_{j_B}\rangle i^{l_B}Y_{l_Bm_{l_B}}(\hat{r})I^B_{Apl_Bj_B}(r),$$

where $\mathcal{A}$ is the antisymmetrization operator, φ is a bound state wave function, ξ is a set of internal coordinates including spin-isospin variables and $\vec{r}$ is the vector connecting the center of mass of nucleus A with p. In the third line, the

antisymmetrization factors have been absorbed in the radial overlap integrals $I(r)$. The multipole expansion is carried out over l_B, j_B values allowed by angular momentum and parity conservation for the partition $B \rightarrow A + p$. Outside the core the antisymmetrization effects are small and the overlap integral behaves very much like the radial wave function for a single particle in the potential given by the core [17], but the overlap integral is not an eigenfunction of the total Hamiltonian, and hence, it is not normalized to unity. The rms radius of the wave function of the last nucleon becomes:

$$r_h^2 = \int_0^\infty r^4 dr I_g^2(r) + \int_0^\infty r^4 dr I_e^2(r) + \cdots = r_g^2 + r_e^2 + \cdots , \tag{1}$$

where $I_g(r)$ and $I_e(r)$ are the overlap integrals arising from the parts of the wave function where the nucleon orbits the ground and excited states of the core, respectively. Inside the core of the nucleus the overlap integral involves many-body functions, and it may be difficult to calculate. At asymptotic distances where nuclear forces are vanishingly small, $r > R_N$, for the proton case, the overlap integral behaves as

$$I^B_{Apl_Bj_B}(r) \rightarrow C^B_{Apl_Bj_B} \frac{W_{-\eta_B, l_B+1/2}(2k_B r)}{r}. \tag{2}$$

Here $C^B_{Apl_Bj_B}$ is the asymptotic normalization coefficient defining the amplitude of the tail of the overlap integral, W is the Whittaker function [18] obtained by solving the Schrödinger equation for two charged particles at negative energy $\epsilon_B = -S_p$, $k_B = \sqrt{-\frac{2\mu_{Ap}\epsilon_B}{\hbar^2}}$ is the wave number, μ_{Ap} is the reduced mass of particles A and p, and η_B is the Sommerfeld parameter for the bound state (Ap). In the case the last nucleon is a neutron, outside the nuclear potential, it only feels the centrifugal barrier, if any, and the Whittaker function essentially becomes a Haenkel function, but the rest of the formalism remains the same. If the asymptotic normalization coefficients $C^B_{Apl_Bj_B}$ can be extracted from any peripheral observable that is measured experimentally, in particular from one-proton or one-neutron transfer reactions, then they can be used to evaluate other observables for which the outer region contributes most. It follows that the halo radius can be correlated to the ANCs in a simple way. To have a clear halo state, a rather pure single particle configuration must dominate the wave function of the last nucleon, and therefore the first term in Eq. (1) dominates. For it we can further write, separating the contributions of the interior and of the asymptotic region:

$$r_g^2 = \int_0^{R_N} r^4 dr I_g^2(r) + C_g^2 \int_{R_N}^\infty r^2 dr W^2(2k_B r) \tag{3}$$

(in the neutron case, the second integrand contains the appropriate Haenkel function and an extra $(k_B r)^2$). We may also note that $I_g(r)$ may have more

than one component, as is the case for the $1p_{3/2}$ and $1p_{1/2}$ components in the ^{8}B case, or $2s_{1/2}$ and $1d_{5/2}$ in the ^{14}B case. For the halo states, the asymptotic region, namely the second term in Eq. (3), contributes most, and we correctly account for this most important term by using the ANC extracted from experiment. Also, instead of totally neglecting the first term that gives the contribution of the interior of the nucleus, we replace it by the single particle approximation

$$I^B_{sp}(r) = S^{1/2}_{nlj}\varphi_{nlj}(r) = \frac{C_{nlj}}{b_{njl}}\varphi_{nlj}(r), \tag{4}$$

where S_{nlj} is the (sometimes not accurately determined) spectroscopic factor and b_{nlj} is the single particle asymptotic normalization coefficient of the normalized single particle radial wave function $\varphi_{nlj}(r)$ calculated in a mean field potential. We show that the particular choice of the potential parameters (and therefore of the overlap integral in the interior of the nucleus) does not alter much the value given by Eq. (3) and the procedure gives a virtually model independent rms radius r_g. In Ref. [13] we used potentials of different shapes: Woods-Saxon, Gaussian, Morse and square-well, and of different geometrical parameters to illustrate this statement. In the following we shall restrict ourselves to Woods-Saxon potentials of different geometries, as enough general to demonstrate our point.

In order to determine the contribution of the asymptotic part of the wave function to the halo radius, we define, as in [13]:

$$D_\lambda(R_N) = \left(\frac{\int_{R_N}^\infty r^{2\lambda}dr\psi^2(r)}{\int_0^\infty r^{2\lambda}dr\psi^2(r)}\right)^{1/\lambda}, \tag{5}$$

with $\lambda = 1, 2$, which measures the contribution of the asymptotic part to the norm and to the rms radius, respectively.

The nuclear rms radius is evaluated according to [19],

$$r^2_m = \frac{1}{A+1}(Ar^2_c + r^2_p + \frac{A}{A+1}r^2_h), \tag{6}$$

where A is the mass number of the core, r_c is the radius of the core, $r_p = 0.8$ fm is the proton radius, and r_h is the halo radius. This formula assumes that the core (A) behaves identically inside the nucleus $(A+1)$ as the free nucleus A. The equation shows that in the limit of large nucleus $(A \gg 1)$, $r_m \approx r_c$ and therefore halo states may appear only in light nuclei. The results for all cases treated below are summarized in Table 1.

Table 1

Halo radii (r_h) deduced from ANC method. The nuclear rms radius (r_m) is evaluated using a cluster formula [19] with core radius r_c fixed to HF values. For ^{8}B the ANC value includes the small admixture from the $p_{1/2}$ component

Nucleus	halo state	$S_{p(n)(MeV)}$	C^2 (fm^{-1})	Ref.	r_h (fm)	r_c (fm)	r_m(fm)
^{8}B	$\pi 1p_{3/2}$	0.137	0.483(50)	[22]	4.62(24)	2.33	2.60(4)
^{11}Be	$\nu 2s_{1/2}$	0.504	0.505(6)	[5]	6.26(46)	2.46	2.96(8)
^{14}B	$\nu 2s_{1/2}$	0.970	1.09(2)	[6]	5.46(26)	2.65	2.85(3)
^{13}C*	$\nu 2s_{1/2}$	1.857	3.65(49)	[33]	5.10(38)	2.42	2.70(5)
^{15}C	$\nu 2s_{1/2}$	1.218	1.48(18)	[34, 7]	5.62(68)	2.59	2.92(8)
^{17}O*	$\nu 2s_{1/2}$	3.272	7.78(49)	[30]	4.24(20)	2.64	2.76(2)
^{17}F	$\pi 1d_{5/2}$	0.600	1.08(10)	[28]	4.45(42)	2.64	2.78(4)
^{17}F*	$\pi 2s_{1/2}$	0.105	6480(680)	[28]	5.56(33)	2.64	2.88(4)
^{21}Na*	$\pi 2s_{1/2}$	0.007	6.8E33	[36]	5.12(38)	2.81	2.96(3)

3. HALO STATES IN NUCLEI

3.1. THE ^{8}B GROUND STATE

This is one of the known candidates for proton halo states. The separation energy of the last proton in this $J^\pi = 2^+$ state is very low, $\epsilon_p = -137$ keV, and it is in a p state. In fact it is a superposition, in an unknown proportion, of a major $1p_{3/2}$ component and a smaller $1p_{1/2}$ component, which have virtually the same asymptotic radial behavior. The asymptotic normalization coefficient for ^{8}B$\rightarrow^7$Be $+p$, specifying the amplitude of the tail of the ^{8}B wave function projected on the two body channel ^{7}Be$+p$, has been determined in several proton transfer experiments induced by radioactive ^{7}Be beams, either on deuteron targets [20] or on heavier targets, using the peripheral proton transfer reactions ^{10}B(^{7}Be,^{8}B)^{9}Be [21] and ^{14}N(^{7}Be,^{8}B)^{13}C [22]. Concerns were voiced about the uncertainties in the DWBA calculations used to extract the ANC from the data on the deuteron target [23, 24], therefore we only choose the ANC extracted from proton transfer reactions on the heavier targets. A more recent analysis [25] of uncertainties in these two reactions yielded a weighted average ANC $C^2_{p_{3/2}} = 0.414 \pm 0.049$ fm^{-1}. In Ref. [13], using an effective ANC value $C_{tot} = 0.670 \pm 0.034$ fm$^{-1/2}$ ($C^2_{tot} = C^2_{p_{3/2}} + C^2_{p_{1/2}}$), we found the rms radius of the proton halo to be $\langle r^2 \rangle^{1/2} = 4.20 \pm 0.22$ fm, barely about twice as large as the rms radius of the ^{7}Be core nucleus $r_c = 2.31 \pm 0.02$ fm [9] Similar values for the ANC were determined from a detailed analysis of all existing ^{8}B breakup data for energies at or above the Fermi energy [26, 27]: $C^2_{tot} = 0.483 \pm 0.050$ fm^{-1}, and, of course, a similar value was extracted for

the rms radius of the halo $\langle r^2\rangle^{1/2} = 4.62 \pm 0.24$ fm. The results obtained for the rms radius depend only on the quantum number of its orbital angular momentum and the separation energy, which are well established, and not at all, or less, on the shape assumed for the proton binding potential and the details of the configuration of the ground state wave function (spectroscopic factors). The effect of the small binding energy of the last proton, which favors a large extent of the wave function in the asymptotic region outside the core, is counterbalanced by the presence of a small proton-core Coulomb barrier and of a centrifugal barrier (p-state), that act together to keep the wave function inside the range of the core. The situation in this nucleus was treated in detail in the previous paper [13], and we include it here for the completeness of the present discussion. Note that the nuclear rms radius given in Table 1 is much larger than the experimental value 2.38±0.04 [9], obtained by Glauber inversion of interaction cross section, suggesting that this method is less sensitive when the few body character of the halo is ignored.

3.2. THE ^{17}F$^*(1/2^+)$ FIRST EXCITED STATE

Another known candidate for a proton halo is the first excited state in ^{17}F, $J^\pi = 1/2^+$, $E_{exc} = 0.495$ MeV. Two factors favor the proton in this state to be even more extended than in the ^{8}B ground state: the binding energy $\epsilon_p = -105$ keV is slightly lower, and it is in a s-wave (no centrifugal barrier). A somewhat larger Coulomb barrier due to the larger atomic number of the core works in the opposite direction. The extra node in the $2s_{1/2}$ wave function can be another complication. We have determined the ANCs for the ground state and for the first excited state in ^{17}F from an ^{16}O(^{3}He,d)^{17}F experiment [28]. A value $C^2(2s_{1/2}) = 6480 \pm 680$ fm^{-1} was obtained for the weakly bound first excited state. We use the same grid procedure as in [13]. The rms radii of the $2s_{1/2}$ single particle wave functions calculated in Woods-Saxon wells adjusted to reproduce the experimental binding energy of the proton, range from 4.69 to 5.57 fm when the well parameters are varied in the reasonable range from $r_0 = 1.0$ to 1.3 fm and $a = 0.50$ to 0.70 fm. However, when we constrain the overlap integrals to have the asymptotic behavior given by the experimental ANC, the average over the 12 points of the (r_0, a) grid becomes $\langle r^2\rangle^{1/2} = 5.56$ fm, with a standard deviation of only 0.16 fm. We stress that this is equivalent with considering correctly the second term in Eq. (3) which contributes most, and replacing the unknown first term that gives the contribution of the region inside the core with the single particle like approximation, rather than totally ignoring it, as explained above. The value of the standard deviation of the calculated rms radii around the average value by this method is about two times smaller than the $\delta\langle r^2\rangle^{1/2} = 0.29$ fm uncertainty in the average value

given by the 5.2% uncertainty of the ANC determination from experiment. Combining the two, we can conclude that the rms radius of the proton halo is $r_h = 5.56 \pm 0.33$ fm. Searching for Woods-Saxon potentials that produce single particle ANCs matching the experimental one (that is, with spectroscopic factor unity; a reasonable assumption for this state), we find $r_{sp} = 5.43$ fm, also within the margin of error. The value obtained is about 2 times larger than the rms radius of the point nucleon distribution for the ^{16}O core $r_c = 2.59$ fm (obtained by subtracting quadratically the proton radius 0.85 fm, from the experimental rms charge radius of Ref. [1]), and therefore, we can conclude that the first excited state in ^{17}F is a clear proton halo state. By evaluating $D_{1(2)}$ of Eq. (5), at different distances, we find that, in average, the last proton is located with 76% probability at radii $r > 3.0$ fm, and this region contributes about 98% to the rms radius. For $r > 5.0$ fm, the numbers are 33% and 84%, respectively, which shows again the dominant contribution of the tail to the rms radius (Fig. 1). In this figure the halo density is defined as $\rho_h(r) = \mathcal{R}^2_{nlj}(r)/4\pi$, where $\mathcal{R}_{nlj}(r)$ is the radial part of the single particle wave function.

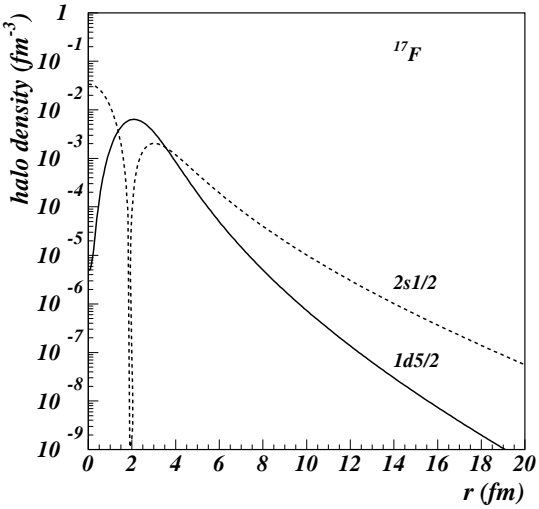

Fig. 1 – Halo density for a proton in ^{17}F for the ground state $J^\pi = 5/2^+$, $E = 0.600$ MeV (blue line) and for excited state $J^\pi = 1/2^+$, $E = 0.105$ MeV (red line). Both densities are normalized to unity. Wave functions are calculated in a Woods-Saxon potential which reproduces the separation energy for a radius fixed at the HF value 2 of the core radius and a diffuseness of 0.6 fm. The difference in the halo amplitudes comes essentially from the combined effect of separation energy and angular momentum of the wave function.

We expect the core excitation to give minimum contribution r_e (Eq. (1)) in this case because the next configuration of the same spin and parity $(2^+ \otimes d_{5/2})1/2^+$ is about 7 MeV higher in the energy spectrum and therefore the mixing must be small. Again, the whole result does not depend on any assumption about the structure of the state or on the single particle potential.

Furthermore, if we try to apply the same procedure to the $5/2^+$ ground state of the same nucleus ^{17}F, we notice that the procedure does not work so well. In Ref. [28] we found for this state the ANC $C^2(1d_{5/2}) = 1.08 \pm 0.10$ fm^{-1}. Using the same grid as above, renormalizing the overlap function to the measured ANC increases, rather than decreases, the spread of the values of the calculated rms radii around the average value $r_h(1d_{5/2}) = 4.45$ fm. The standard deviation is 0.42 fm, twice larger than the uncertainty due to the experimental uncertainty in the determination of the ANC. Also the value is much larger than the s.p. estimate of $r_{sp} = 3.70$ fm. The asymptotic part of the wave function makes a significant contribution to the rms radius, but it does not dominate as in the case of the first excited state (Fig. 1, bottom). The reasons are both the larger proton binding energy and the larger orbital angular momentum of this state which produces a centrifugal barrier that tends to keep the radial wave function in the interior.

The large size of the first excited state $J^\pi = 1/2^+$ in ^{17}F was recognized earlier by Morlock *et al.* from their radiative proton capture measurement at low energies [29]. They use a careful folding procedure of the target matter distribution with a DDM3Y effective interaction, and scale it to reproduce the experimental binding energies of both $1d_{5/2}$ and $2s_{1/2}$ orbitals, to obtain a potential well with rms radius $R_F = 3.31$ fm. With an assumed spectroscopic factor equal to unity they calculate the rms radius of the loosely bound proton in the $1/2^+$ state at $r_h(1/2^+) = r_{sp}(2s_{1/2}) = 5.33$ fm, a value very close to what we obtained above without any assumptions about the structure of the state (spectroscopic factor or shape of the single particle potential) other than the orbital angular momentum and the value of the proton separation energy, and the experimental ANC.

3.3. THE MIRROR STATE IN ^{17}O*$(1/2^+)$

The corresponding state in the one neutron nucleus ^{17}O was studied by (d,p) experiments at several energies, but these are not always peripheral reactions. It was also studied in a ^{16}O(^{4}He,^{3}He)^{17}O measurement [30]. Using these measurements and a DWBA analysis we extracted an ANC $C^2(2s_{1/2}) = 7.78$ fm^{-1} for the $J^\pi = 1/2^+$ state at $E_{exc} = 0.871$ MeV, and consequently a rms radius $\langle r^2 \rangle^{1/2} = 4.24$ fm, much smaller than that of its mirror state in ^{17}F. The absence of the Coulomb repulsion energy, compared to ^{17}F, plays here a

double role, pushing in competing directions. First it makes the separation energy of the last neutron to be much larger: $S_n = -\epsilon_n = 3.272$ MeV, and therefore contributes toward keeping the neutron bound closer to the core. Second, there is no Coulomb and no centrifugal barrier to prevent the wave function of this state to extend far outside the nuclear core. To evaluate these two effects we vary them one at the time. If we force the proton to have the same binding energy as the neutron $\epsilon_p = \epsilon_n = -3.272$ MeV, the rms radius of the corresponding single proton wave function shrinks from 4.26 fm to 3.90 fm (not much!). Alternatively, an s neutron at the binding energy of proton state in ^{17}F will have a rms radius of 12.1 fm, a much larger increase. It appears that the presence of the Coulomb barrier is more important than the role of the binding energy. Ref. [31] compare these two mirror states in ^{17}F and ^{17}O, both good (= rather pure) single particle states, and observe that the Coulomb barrier is the important factor that determine their sizes.

3.4. ^{11}Be GROUND STATE

^{11}Be was one of the first examples of large one neutron halo as demonstrated by interaction cross section measurements [4]. Total reaction cross section, core like fragment parallel momentum distributions, as well as separate contributions to the inclusive cross section coming from stripping and diffraction dissociation have been measured by Negoita *et al.* [32] using the telescope method, providing thus a useful test for eikonal type models of reaction mechanism. More recently, Aumann *et al.* [5] studied the breakup reaction ^{9}Be(^{11}Be,^{10}Be+γ)X at 60 MeV/nucleon and found that the ground state structure of the ^{11}Be is dominated by the intruder state $2s_{1/2}$ (80%) and a small admixture $1d_{5/2}$ (20%) from core excited state. Using their data and our Glauber model to calculate one-neutron knockout reaction cross sections, we find a rms radius $\langle r^2\rangle^{1/2} = 6.26 \pm 0.46$ fm for the ground state of ^{11}Be, the largest radius of all cases included in Table 1. This is due to the favorable combination of all three factors contributing: is a neutron state (no Coulomb barrier), is mostly a $2s_{1/2}$ state (no centrifugal barrier), and has a relatively small binding energy ($S_n = 0.504$ MeV).

3.5. The ^{13}C$^*(1/2^+)$ FIRST EXCITED STATE

Next we use the procedure for the first excited state in ^{13}C, $J^\pi = 1/2^+$, $E_{exc} = 3.089$ MeV. It has a somewhat large binding energy $S_n = 1.857$ MeV, but is also a neutron $2s_{1/2}$ state and, therefore, benefits from lacking a

Coulomb or a centrifugal barrier. This state plays an important role in the determination of the cross section for the neutron radiative capture ^{12}C(n,γ)^{13}C at astrophysical energies. The ANC for this state was determined from a ^{12}C(d,p) experiment at $E_d = 11.8$ MeV at the University of Tokyo to be $C^2 = 3.65 \pm 0.49$ fm^{-1} [33]. They show explicitly in Fig. 3 that using the ANC parametrization the result does not depend (less than 1% variation) on the parameters of the Woods-Saxon potential used to calculate the bound state wave function of the transferred neutron, whereas in the alternative parametrization with the spectroscopic factor, the values extracted may differ by up to 45%. If we use radial overlap integrals that have the asymptotic behavior given by the experimental ANC, we obtain an rms radius $\langle r^2 \rangle^{1/2} = 5.10 \pm 0.38$ fm. This is a good argument that it is a neutron halo state, because it is again more than a factor two larger than the point particle rms radius of the ^{12}C

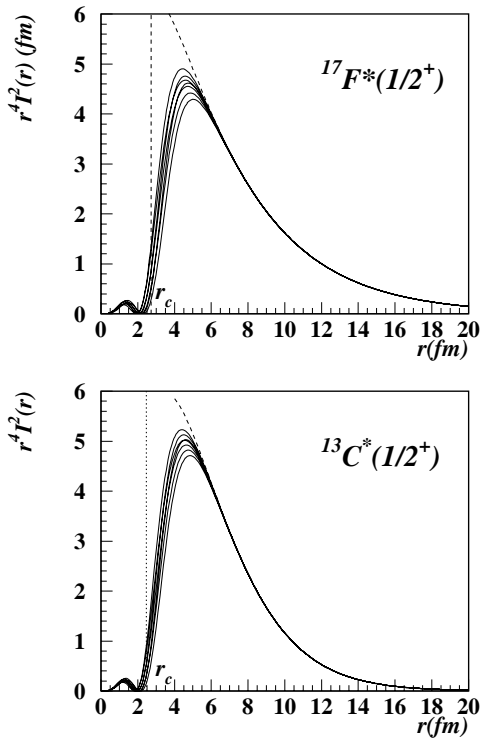

Fig. 2 – The overlap integral in the single particle approximation for a $2s_{1/2}$ neutron halo state (in ^{13}C*)and a proton halo state (in ^{17}F*) as a function of radial distance r. The vertical dotted line indicate the physical dimension of the core. The spread of the w.f. in the nuclear interior reflects the uncertainty in the geometry of the single particle potential. In the external region the w.f. match perfectly the Whittaker function (dashed line).

core (r_c = 2.32 fm). In Fig. 2 we compare the density distributions for the $2s_{1/2}$ states in ^{17}F* (proton state, S_p = 105 keV) and ^{13}C (neutron state, S_n = 1.857 MeV). The distributions are similar, and we see again that the lack of any Coulomb or centrifugal barrier is important in producing this halo state, despite a not so low separation energy for the neutron state.

3.6. THE ^{15}C GROUND STATE

Another interesting example is that of the ^{15}C ground state. For this nucleus we have extracted the ANC from the absolute cross section for the one neutron breakup of 54 MeV/nucleon ^{15}C on a carbon target, leading to the g.s. and first excited state of ^{14}C [7, 34]. The nucleus has a relatively small neutron binding energy of S_n = 1.218 MeV and the spin and parity of the state are proved to be $J^\pi = 1/2^+$, mostly a neutron in a $2s_{1/2}$ orbital coupled to the ground state of the ^{14}C core. Comparing the breakup data with Glauber model calculations we found $C^2 = 1.48 \pm 0.18$ fm^{-1} [35]. Again, the use of the ANC, in both analysis of the breakup data and the determination of the rms radius, avoids unnecessary uncertainties due to the geometry of the core-neutron bining potential, not well known for this neutron-rich nucleus. With the ANC extracted we determine the rms radius of the outer neutron to be $\langle r^2 \rangle^{1/2} = 5.62 \pm 0.68$ fm, more than twice as large than the radius of the core r_c = 2.59 fm. We remind that as everywhere in this paper, the error quoted includes any systematic uncertainty arrising from the choice of the model parameters.

3.7. THE THIRD EXCITED STATE IN ^{21}Na ($1/2^+$)

This is a very interesting example because the binding energy of this proton state is extremely small. Proton single-particle states in ^{21}Na were studied in a careful ^{20}Ne(d,n)^{21}Na experiment at E_d = 25 MeV [36]. The data are compared with DWBA calculations or with calculations with the adiabatic deuteron (Fig. 3) breakup approximation [37].

The third excited state has an excitation energy E_{exc} = 2424.9(7) keV (most precise value from gamma ray decay measurements [38]) and the proton separation energy for the ground state is S_p = 2431.3(7) keV. It follows that the proton binding energy for this state is $S'_p = (S_p - E_{exc})$ = 6.4 keV. Energetically speaking, this state is just barely bound. The analysis of the (d,n) angular distribution gives a clear $l = 0$ assignment and the absolute value of the cross section shows that the state has an almost pure single particle $2s_{1/2}$ configuration. The corresponding Whittaker function in Eq. (2) is very small

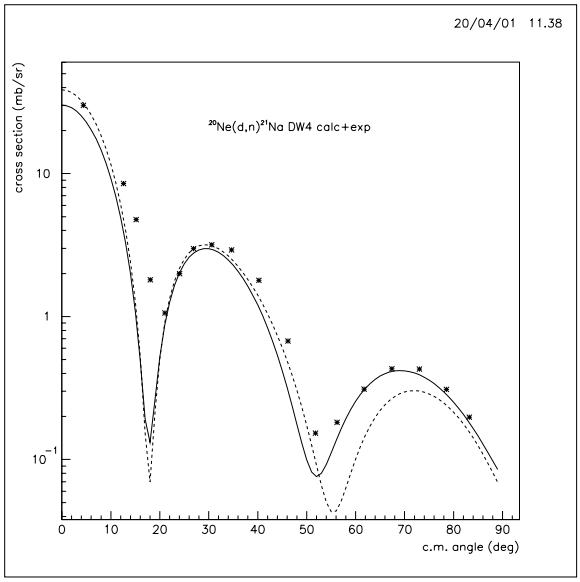

Fig. 3 – DWBA calculation for the proton transfer reaction ^{20}Ne(d,n)^{21}Na at E_d=25 MeV. Experimental data taken from ref. [36].

due to a large Sommerfeld parameter $\eta = 19.25$. This leads to a very large ANC for this state $C(2s_{1/2}) = 8.25e16$ fm$^{-1/2}$. However the rms radius found for this state is $\langle r^2\rangle^{1/2} = 5.12 \pm 0.38$ fm, a value which is large compared with the point rms radius of the core nucleus ^{20}Ne $r_c = 2.88$ fm, but not even twice as large. The very low binding energy is not enough to make the size of this state explode! However if we drop the Coulomb interaction, a neutron state in the same potential, with the same binding energy of 6.4 keV would extend very far, with a rms radius $r_n = 72$ fm (and easier to evaluate analytically than numerically, due to the very large range needed (≈ 500 fm) for the convergence of the numerical calculation). This is essentially the same conclusion as that from the ^{17}F and ^{17}O comparison, above. It is easy to explain by the fact that the asymptotic behavior of the radial wave function is very different in the two cases:

$$\varphi(r) \simeq C\frac{e^{-kr}}{r}\ (n)\ \simeq \frac{C}{(2k)^\eta}\frac{e^{-kr}}{r^{\eta+1}}\ (p). \tag{7}$$

When the separation energy is small, the neutron wave function drops very slowly, due to the exponential factor, but on the contrary, for the same binding energy, the asymptotic radial behavior of the proton wave function is dictated by the $r^{-\eta}$ factor, and it falls rapidly out, because the Sommerfeld parameter η increases with decreasing binding energy (Fig. 4). This keeps the rms radius relatively small, no matter what the separation energy is, and the

examples above in ^{17}F and ^{21}Na are very clear illustrations of this phenomenon. Further discussion is given bellow in Section 4. This is the main reason why there are not so many proton halo nuclei, except for the two classical examples ^{8}B g.s. and ^{17}F first excited state, whereas examples of neutron halo nuclei are plenty.

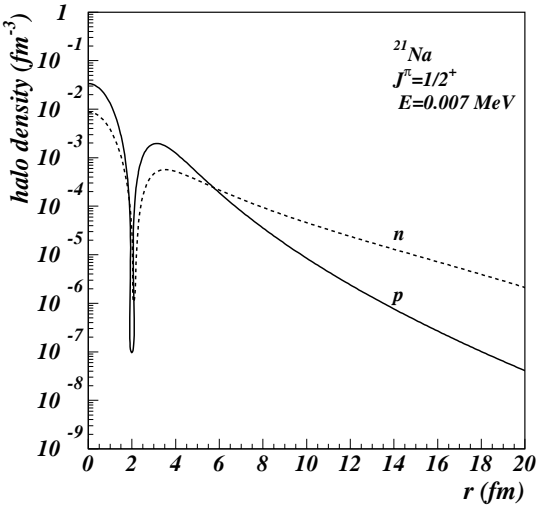

Fig. 4 – (Color on line) Halo density for a proton (blue line) and neutron (red line) in ^{21}Na for a $2s_{1/2}$, $S_{n(p)} = 0.007$ MeV state. Both densities are normalized to unity. Wave functions are calculated in a Woods-Saxon potential which reproduces the separation energy with a radius fixed at the measured value of the core [9] and a diffuseness of 0.6 fm.

The important factor in the proton state is therefore the Coulomb barrier which squeezes the wave function inside the core region, or close to it. The corresponding $1/2^+$ state in the isotope nucleus with two extra neutrons ^{23}Na has a proton binding energy of $\epsilon_p = 6.403$ MeV, and the size of the orbital is squeezed down to $r_h = 3.60$ fm.

4. PROTON HALO AT ZERO ENERGY

In the previous sections we estimated the rms for proton and neutron halo orbitals. We expect that, while the the rms for proton halo nuclei remains constrained when the binding energy $\varepsilon \to 0$, the rms of the neutron halo orbitals rapidly increases when binding energy decreases.

In this section we present a simple qualitative explanation of the different behavior of the rms for proton and neutron halo orbitals. The physical reason

is a very simple: the Coulomb barrier constrains the proton rms. We demonstrate it below. The rms of the nucleon orbital is given by Eq. (1). Without loosing generality we restrict ourselves to s-wave orbitals for simplicity.

The halo neutron rms is given by

$$r_g^2(ext) = \int_0^\infty \mathrm{d}r\, r^4\, \varphi^2(r) = \int_0^{R_N} \mathrm{d}r\, r^4\, \varphi^2(r) + b^2 \int_{R_N}^\infty \mathrm{d}r\, r^2\, e^{-2\,\kappa\, r}$$
$$\approx b^2 \int_{R_N}^\infty \mathrm{d}r\, r^2\, e^{-2\,\kappa\, r}. \tag{8}$$

It consists of two contributions, internal and external. Internal contribution gives a small contribution and, for our purposes, can be neglected, so it is enough to consider only the external part. For simplicity we dropped the quantum numbers specifying the halo state. We assume that the halo state is approximated by a single-particle wave function, i.e. its spectroscopic factor is close to one. Then according to Eq. (4) the asymptotic normalization coefficient $C \approx b$. The nuclear interaction radius R_N is similar to the channel radius in the R-matrix approach and is defined so that at $r = R_N$ the neutron radial bound-state wave function, $\varphi(r)$, can be approximated by its asymptotic term:

$$\varphi(r) \approx b\, e^{-\kappa\, r}/r. \tag{9}$$

R_N depends on the binding energy of the neutron. For example, if the single-particle potential is taken in the Woods-Saxon form, then R_N is choosen to satisfy,

$$V_0\, \frac{1}{1 + e^{(R_N - R)/a}} < \varepsilon. \tag{10}$$

Here, V_0 is the depth of the potential, R and a are the radius and diffuseness, ε is the binding energy. The radius R_N is close to the nuclear radius. From Eq. (10) we get that

$$R_N \sim R + a\, \ln \frac{V_0}{\varepsilon}. \tag{11}$$

Thus, R_N increases logarithmically when ε decreases.

We can estimate now the single-particle asymptotic normalization coefficient b:

$$b^2 = \frac{1 - \int_0^{R_N}\, dr\, r^2\, \psi^2(r)}{\int_{R_N}^\infty\, d\, r\, e^{-2\,\kappa\, r}} = 2\,\kappa\, e^{2\,\kappa\, R_N}. \tag{12}$$

This equation follows from the normalization condition of the bound state wave function. Then we get

$$r_g(exp) = \frac{1}{2\,\kappa^2}\, [2\,\kappa^2\, R_N^2 + 2\,\kappa\, R_N + 1] \left[1 - \int_0^{R_N}\, dr\, r^2\, \psi^2(r)\right]. \tag{13}$$

For $\kappa \to 0\, r_g \to \infty$. Note that $r_g(exp)$ does not depend on the exponential factor $exp(-2\,\kappa\, R_N)$.

(2) The rms of the proton halo orbital is governed by the Coulomb interaction and for small binding energies is given by:

$$r_g = \int_0^{R_N} dr\, r^4\, \varphi^2(r) + b^2 \int_{R_N}^{\infty} dr\, r^2\, [W_{-\eta_f,\,1/2}(2\,\kappa\, r)]^2. \tag{14}$$

Here,

$$\eta = \frac{Z_A e^2\, \mu Ap}{\kappa}, \tag{15}$$

is the Coulomb parameter for the bound state, $Z_A e$ is the charge of the target A, μ_{Ap} is the reduced mass of the proton and the target. Using the normalization condition for the proton bound state wave function we get

$$b^2 = \frac{1 - \int_0^{R_N} dr\, r^4\, \varphi^2(r)}{\int_{R_N}^{\infty} dr\, [W_{-\eta_f,\,1/2}(2\,\kappa\, r)]^2}. \tag{16}$$

The halo proton rms behaves differently than the neutron one when binding energy ε decreases. While neutron halo rms increases the proton rms remains confined by the Coulomb field. We have demonstrated it performing numerical calculations (Fig. 5) and here we give a qualitative explanation of such a

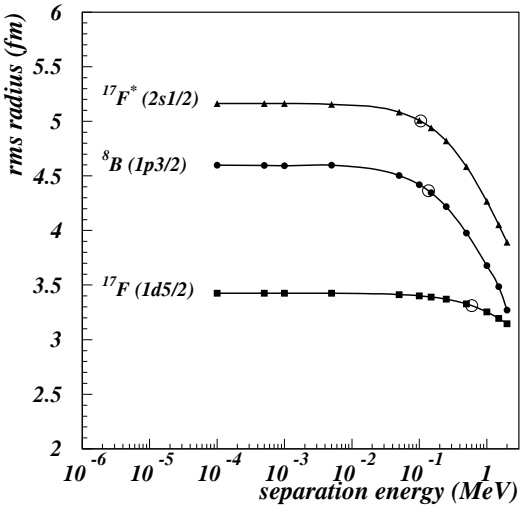

Fig. 5 – Simulation of the dependence of the rms radius of a proton halo state versus separation energy, suggesting the saturation effect at zero energy. Open circles indicate the rms radius at the physical separation energy.

behavior. Due to the presence of the r^4-factor in the first integral in Eq. (14) the contribution of the first term is small. The second integral represents the external contribution to the halo proton rms. For small enough κ the Coulomb

parameter $\eta \gg 1$ and the convergence of the second integral is defined by the denominator $1/r^{\eta}$ rather than by the exponential factor. At large enough r, in the region defining the convergence of the integral in Eq. (14) we can use the asymptotic expansion for the Whittaker function [18] for the s-wave:

$$W_{-\eta_f,\,1/2}(2\,\kappa\,r) = \frac{e^{-\kappa\,r}}{(2\,\kappa\,r)^{\eta_f}} \left\{ \sum_{j=0}^{\infty} \frac{(l_f - \eta_f)_j\ (\eta_f + j)_j}{j!\ (2\,\kappa\,r)^j} \right\}. \qquad (17)$$

The first asymptotic term of the Whittaker function is defined not only by the exponential term $e^{-\kappa\,r}$ but also the Coulomb barrier factor $1/r^{\eta_f}$. For small binding energies and large enough charges the Coulomb barrier factor $1/r^{\eta_f}$, rather than the exponential factor, which provides a sharp decrease of the Whittaker function when r increases. This Coulomb barrier factor becomes the decisive one which governs the convergence of the integral in Eq. (14) and just this Coulomb barrier factor keeps the rms of the proton halo limited. For a very qualitative explanation of the external term of the rms behavior we can assume that r^2 is a smooth function compared to a sharply dying $[W_{-\eta_f,\,1/2}(2\,\kappa\,r)]^2$. Then taking r^2 out of the integral at $r = R_N$ and allowing for Eq. (16) we get

$$r_g(ext) = b^2 \int_{R_N}^{\infty} dr\, r^2\, [W_{-\eta_f,\,1/2}(2\,\kappa\,r)]^2 \approx R_N^2\, [1 - \int_0^{R_N} dr\, r^4\, \varphi^2(r)] \qquad (18)$$

and

$$r_g \approx \int_0^{R_N} dr\, r^4\, \varphi^2(r) + R_N^2\, [1 - \int_0^{R_N} dr\, r^4\, \varphi^2(r)]. \qquad (19)$$

Thus, the halo proton rms is limited when the proton binding energy decreases in sharp contrast to the halo neutron rms behavior.

5. CONCLUSIONS

The experimental asymptotic normalization coefficient (ANC) specifying the amplitude of the tail of the many body wave function was used to calculate the rms radius of various halo states in light nuclei. We showed that for halo nuclear states, the asymptotic region has the dominant contribution to observables favoring large distances from the core, like the rms radius, and therefore the ANC is the most relevant quantity to be extracted from the data. In particular we have shown that the ANC method gives reliable and almost model independent rms values. The method does not depend on the spectroscopic factors of the states or on the details of the potential wells assumed in the usual single particle description. This may become particularly important for light, weakly bound nuclei near the drip line where major uncertainties

about the mean field approach exists. A variety of ground and excited states have been studied, pointing to the important role of the Coulomb barrier, separation energy and angular momentum in the developpement of a halo.

Acknowledgement. This work was supported by Cyclotron Institute, Texas A &M Univ. and by National Authority for Scientific Research (Romania), grand M3-165/2006.

REFERENCES

1. H. de Vries, C.W. de Jaeger, and C. de Vries, At. Data and Nucl. Data Tables, **36**, 495 (1987).
2. I. Angeli, At. Data and Nucl. Data Tables, **87**, 185 (2004).
3. B.A. Brown, Phys. Rev. Lett., **85**, 5296 (2000).
4. I. Tanihata, T. Kobayashi, O. Yamakawa, S. Shimoura, K. Ekuni, K. Sugimoto, N. Takahashi and T. Shimoda, Phys. Lett., **B206**, 592 (1988).
5. T. Aumann *et al.*, Phys. Rev. Lett., **84**, 35 (2000).
6. V. Guimares *et al.*, Phys. Rev., **C 61**, 064609(2000).
7. E. Sauvan *et al.*, Phys. Lett., **B 491**, 1 (2000).
8. I. Tanihata, J. Phys. G: Nucl. Part. Phys., **22**, 157 (1996).
9. A. Ozawa, T. Suzuki, I. Tanihata, Nucl. Phys., **A 693**, 32 (2001).
10. T. Suzuki *et al.*, Nucl. Phys., **A 630**, 661 (1998).
11. A. Ozawa *et al.*, Nucl. Phys., **A 691**, 599 (2001).
12. J.S. Al-Khalili, J.A. Tostevin, I.J. Thompson, Phys. Rev., **C 54**, 1843 (1996).
13. F. Carstoiu, L. Trache, C.A. Gagliardi, A.M. Mukhamedzhanov and R.E. Tribble, Phys. Rev., **C 63**, 054310 (2001).
14. A. Azhari, V. Burjan, F. Carstoiu, C.A. Gagliardi, V. Kroha, A.M. Mukhamedzhanov, X. Tang, L. Trache and R.E. Tribble, Phys. Rev., **C 63**, 055803 (2001).
15. G.R. Satchler, *Direct Nuclear Reactions*, Clarendon Press, Oxford Univ. Press, N.Y., 1983.
16. H.M. Xu, C.A. Gagliardi, R.E. Tribble, A.M. Mukhamedzhanov and N.K. Timofeyuk, Phys. Rev. Lett., **73**, 2027 (1994).
17. A.M. Mukhamedzhanov, C.A. Gagliardi and R.E. Tribble, Phys. Rev., **C 63**, 024612 (2001).
18. M. Abramowitz and I. Stegun, *Handbook of Mathematical Functions*, Dover Publ., Inc., N.Y.
19. B. Buck and A.A. Pilt, Nucl. Phys., **A 280**, 133 (1977).
20. W. Liu *et al.*, Phys. Rev. Lett., **77**, 611 (1996).
21. A. Azhari, V. Burjan, F. Carstoiu, H. Dejbakhsh, C.A. Gagliardi, V. Kroha, A.M. Mukhamedzhanov, L. Trache and R.E. Tribble, Phys. Rev. Lett., **82**, 3960 (1999).
22. A. Azhari, V. Burjan, F. Carstoiu, C.A. Gagliardi, V. Kroha, A.M. Mukhamedzhanov, X. Tang, L. Trache and R.E. Tribble, Phys. Rev., **C 60**, 055803 (1999).
23. C. Gagliardi, A.M. Mukhamedzhanov, R.E. Tribble, and H.M. Xu, Phys. Rev. Lett., **80**, 421 (1998).
24. J.C. Fernandes, R. Crespo, F.M. Nunes and I.J. Thompson, Phys. Rev., **C 59**, 2865 (1999).

25. G. Tabacaru, A. Azhari, J. Brinkley, V. Burjan, F. Carstoiu, C. Fu, C.A. Gagliardi, V. Kroha, A.M. Mukhamedzhanov, X. Tang, L. Trache, R.E. Tribble and S. Zhou, Phys. Rev., **C 73**, 025808 (2006).
26. L. Trache, F. Carstoiu, C.A. Gagliardi, R.E. Tribble, Phys. Rev. Lett., **87**, 271102 (2001).
27. L. Trache, F. Carstoiu, C.A. Gagliardi, R.E. Tribble, Phys. Rev., **C 73**, 032802(R) (2004).
28. C.A. Gagliardi et al., Phys. Rev., **C 59**, 1149 (1999).
29. R. Morlock, R. Kunz, A. Mayer, M. Jaeger, A. Mueller, J. W. Hammer, P. Mohr, H. Oberhummer, G. Staudt and V. Koelle, Phys. Rev. Lett., **79**, 3837 (1997).
30. M. Yasue, T. Hasegawa, S.I. Hayakawa, K. Ieki, J. Kasagi, S. Kubono, T. Murakami, K. Nisimura, K. Ogawa, H. Ohnuma, R.J. Peterson, H. Shimizu, M.H. Tanaka, and H. Toyokawa, Phys. Rev., **C 46**, 1242 (1992).
31. R. Lewis and A.C. Hayes, Phys. Rev., **C 59**, 1211 (1999).
32. F. Negoita *et al.*, Phys. Rev., **C 59**, 2082 (1999).
33. N. Imai, N. Aoi, S. Kubono, D. Beaumel, K. Abe, S. Kato, T. Kubo, K. Kumagai, M. Kurokawa, X. Liu, A. Mengoni, S. Michimasa, H. Ohnuma, H. Sakurai, P. Strasser, T. Teranishi and M. Ishihara, *Proceedings of the International Topical Conference on Nuclei in the Cosmos*, Aarhus, Denmark, 27 June 2000, Nucl. Phys., **A688**, 281c (2001).
34. V. Maddalena *et al.*, Nucl. Phys., **A 682**, 332c (2001).
35. L. Trache *et al.*, in *Progress in Research*, Apr. 2001-Mar. 2002, Cyclotron Institute, Texas A&M University, p. 1-16.
36. A. Terakawa, T. Tohei, T. Nakagawa, A. Sato, J. Takamatsu, M. Mori, A. Narita, *et al.*., Phys. Rev., **C 48**, 2775 (1993).
37. G.L. Wales and R.C. Johnson, Nucl. Phys., **A 274**, 168 (1978).
38. R.B. Firestone and V.S. Shirley, Eds., *Table of Isotopes*, eighth edition, J. Willey& Sons, New York, 1996.